Chinese Chemical Letters 35 (2024) 109123

Contents lists available at ScienceDirect

Chinese Chemical Letters

journal homepage: www.elsevier.com/locate/cclet

Phosphorus-silicon-integrated electrolyte additive boosts cycling performance and safety of high-voltage lithium-ion batteries

Mei-Chen Liu, Qing-Song Liu, Yi-Zhou Quan, Jia-Ling Yu, Gang Wu*, Xiu-Li Wang*, Yu-Zhong Wang

The Collaborative Innovation Center for Eco-Friendly and Fire-Safety Polymeric Materials (MoE), National Engineering Laboratory of Eco-Friendly Polymeric Materials (Sichuan), State Key Laboratory of Polymer Materials Engineering, College of Chemistry, Sichuan University, Chengdu 610064, China

ARTICLE INFO

Article history:
Received 23 July 2023
Revised 29 August 2023
Accepted 18 September 2023
Available online 22 September 2023

Keywords:
Electrolyte additive
NCM
Lithium-ion batteries
Safety
Cathode-electrolyte interface

ABSTRACT

Safety and energy density are significant for lithium-ion batteries (LIBs), and the flammable organic electrolyte is one of the most critical causes of the safety problem of LIBs. Although $LiNi_{0.8}Co_{0.1}Mn_{0.1}O_2$ (NCM811) cathode with high capacity can improve the energy density, the interface stability between NCM811 cathode and electrolytes needs to be improved. Herein, we report a multifunctional additive, diethyl(2-(triethoxysilyl)ethyl)phosphonate (DETSP), which can suppress the flammability of the electrolyte and enhance the cycling stability of NCM811 cathode with a capacity retention of 89.9% after 400 cycles at 1 C, while that of the blank electrolyte is merely 61.3%. In addition, DETSP is compatible well with the graphite anode without impairing the electrochemical performances. Significantly, the performance and safety of NCM811/graphite full cells are also improved. Experimental and theoretical results demonstrate that DETSP can scavenge acidic byproducts and is beneficial to form a stable cathode-electrolyte interface (CEI). Accordingly, DETSP can potentially be an effective solution to ameliorating the safety of the commercial electrolyte and improving the stability of high-voltage cathodes.

Lithium-ion batteries (LIBs) have achieved great success, widely used in various fields like energy storage, portable devices, and electric vehicles in the past 30 years [1–3]. However, their safety and energy density require further improvement for more advanced and larger scale applications [4]. Due to high capacity and rate capability, nickel-rich layered oxides ($LiNi_{1-x-y}Mn_xCo_yO_2$, Ni-rich NCMs) served as the substitute of conventional cathodes like $LiFePO_4$ and $LiCoO_2$ have attracted much attention, especially $LiNi_{0.8}Co_{0.1}Mn_{0.1}O_2$ (NCM811), which has lower cost and higher energy density owing to its high content of nickel [5–7]. Nevertheless, the cycle stability and safety of NCM811 are limited by the unstable cathode-electrolyte interface (CEI) which often leads to side reaction with electrolyte and further transition metal (TM) dissolution [8,9].

Composed of $LiPF_6$ salt and several kinds of carbonates including dimethyl carbonate (DMC), ethyl methyl carbonate (EMC) and ethylene carbonate (EC), commercial electrolytes usually fail to produce stable CEI at a high voltage besides the high volatility and flammability [10]. An effective way to improve the interfacial stability between commercial electrolytes and high-voltage cathodes is coating the cathode surfaces with inert compounds such as AlF_3 [11] and SiO_2 [12]. However, the coating process not only raises the cost, but also increases the impedance, which leads to low ion conductivity [13]. Comparatively, it is more convenient and cost-efficient to modify the electrolytes with additives [14]. Researchers have reported a host of electrolyte additives which can be oxidized preferentially to form stable CEI due to their higher energy level of the highest occupied molecular orbital (HOMO) than the components of the electrolyte [15–19]. In particular, Si-based additives, such as methoxytriethyleneoxypropyltrimethoxysilane (MTE-TMS) [13], tris(trimethylsilyl)phosphite (TMSP) [18], (2-allyl-phenoxy)trimethylsilane (APTS) [20], and 2,2,7,7-tetramethyl-3,6-dioxa-2,7-disilaoctane-4,4,5,5-tetracarbonitrile (TDSTCN) [21], have been reported to be capable of forming a protective film and effective in inhibiting the capacity decay by scavenging HF to avoid side reactions. Nevertheless, besides improving cycling stability, it is also highly desired for high-voltage LIBs to enhance the safety.

One of the major safety issues of LIBs is the high flammability of carbonate electrolytes. To address this problem, gel polymer electrolytes (GPEs) [22–24] or all solid-state electrolytes (SSEs) [25–27] have been developed. However, these alternatives have their own drawbacks such as complex preparation process, high

* Corresponding authors.
E-mail addresses: gangwu@scu.edu.cn (G. Wu), wangxiuli@scu.edu.cn (X.-L. Wang).

https://doi.org/10.1016/j.cclet.2023.109123
1001-8417/

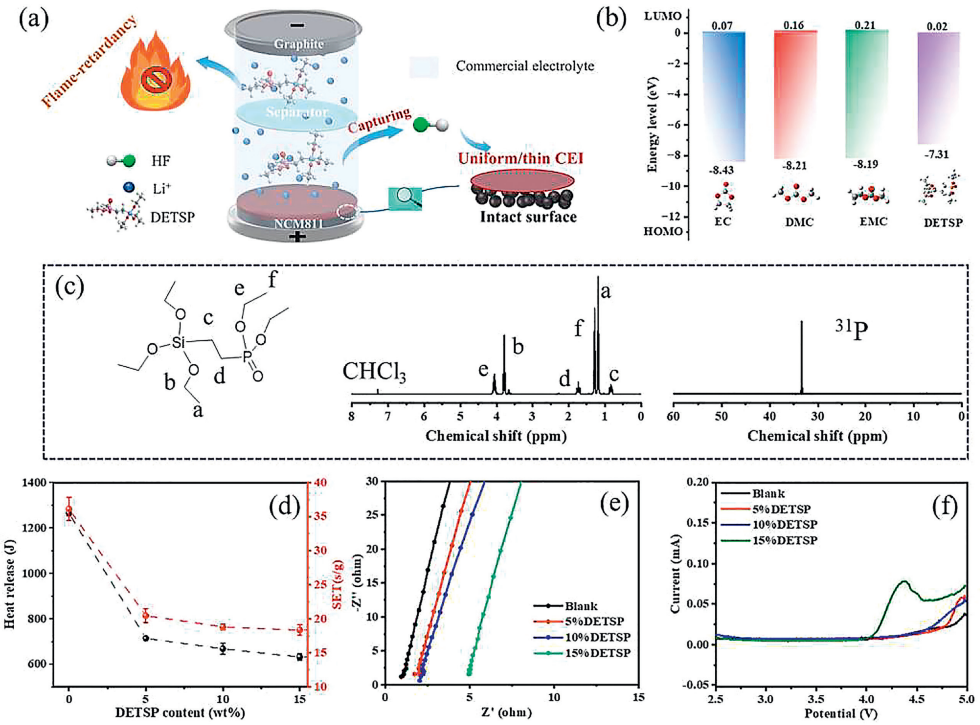

Fig. 1. (a) Schematic diagram of the multifunctional DETSP used in the LIBs. (b) Calculated HOMO/LUMO energy of EC, DMC, EMC, and DETSP. (c) The ^{1}H and ^{31}P NMR spectra of DETSP. (d) SET and total heat release of electrolytes with different contents of DETSP. (e) Nyquist plots and (f) LSV curves of electrolytes with different DETSP contents.

cost, and low conductivity. A more straightforward and cost-effective approach is to add flame retardants to the liquid electrolytes [28,29]. Owing to low cost and low toxicity, the organic phosphorus flame retardants have been widely investigated for their ability to suppress the flammability of the electrolyte [30–36]. Unfortunately, most of the phosphorus retardants are harmful to electrochemical performances, especially unable to passivate the electrodes, which makes electrolytes decompose continuously. Silanes can also serve as flame retardants to improve the safety of electrolytes [37–39], but the flame-retardant efficiency is often inferior to the phosphorus compounds.

To resolve the conflicts between flame retardancy and electrochemical performances, some multifunctional additives have been investigated. Zhu *et al.* [4] reported diethyl(thiophen-2-ylmethyl)phosphonate as a multifunctional additive to suppress the flammability of the electrolyte and simultaneously boost the capacity retention of $LiNi_{0.5}Mn_{1.5}O_4$. Chen *et al.* [37] demonstrated that vinyltriethoxysilane can enhance the cycling stability of $LiCoO_2$ and reduce the self-extinguishing time (SET) of electrolytes. Although some progress has been made, these additives yet suffer from limitations such as complicated synthesis process and inadequate flame retardancy.

In this work, as illustrated in Fig. 1a, we designed a multifunctional additive, *i.e.*, diethyl(2-(triethoxysilyl)ethyl)phosphonate (DETSP), which contains phosphorus and silicon to simultaneously improve the flame retardancy of electrolytes and high electrochemical performance of different electrodes. DETSP is effective in reducing the flammability of commercial electrolytes, and with only 10 wt% of DETSP added, the SET value can be reduced by nearly half. In addition, DETSP is simultaneously compatible with the GP anode and NCM811 cathode, particularly enhancing the cycle stability of NCM811 due to the preferential oxidation to form a protective film and the ability to suppress metal dissolution and phase transition. The cycle performance of full NCN811/GP cells was also improved. DETSP could be a promising multifunctional additive for LIBs to improve both the safety and electrochemical performance, broadening the application fields of LIBs.

The synthesis process of DETSP was shown in Scheme S1 (Supporting information), and the structure of DETSP was characterized by nuclear magnetic resonance (NMR) and mass spectrometry (MS). The ^{1}H NMR and ^{31}P NMR spectra (Fig. 1c) showed that the peaks were all in accordance with the structure of DETSP. The $[M+H]^+$ peak was also consistent with the theoretical value, further confirmed the successful synthesis of DETSP. The oxidation and reduction behaviors can be roughly evaluated by the energy levels of HOMO and the lowest unoccupied molecular orbitals (LUMO) [40]. As shown in Fig. 1b, DETSP has a lower energy level of LUMO and a higher energy level of HOMO, which means that DETSP would reduce and oxidize before the solvents of the commercial electrolytes. The details of relevant experiments will be further discussed later.

The thermogravimetric analysis (TGA) of DETSP was given in Fig. S1 (Supporting information). It can be seen that the temperature at a weight loss of 5% ($T_{5\%}$) was 123.1 °C, which can match the burning process of the blank electrolyte (1 mol/L $LiPF_6$ in EC, DMC, and EMC, 1:1:1 by volume) [41], suggesting that DETSP would be efficient in flame retarding of the blank electrolyte. The SET value is commonly used to characterize the flammability of electrolytes. As shown in Fig. 1d, adding DETSP to the blank electrolyte can significantly reduce its SET value. Specifically, the SET values of the electrolytes with 5% and 10% of DETSP were 20.5 and 18.8 s/g, respectively, lower than that of the blank electrolyte (36.1 s/g), reflecting that the 10% DETSP electrolyte was less flammable [42]. In addition, adding DETSP to the blank electrolyte reduced its heat of combustion by nearly half, further demonstrating that DETSP can effectively reduce its flammability.

The Nyquist plots and linear scanning voltage (LSV) curves of electrolytes with different contents of DETSP were presented in Figs. 1e and f, respectively, and the corresponding ion conductivities and electrochemical windows were summarized in Table

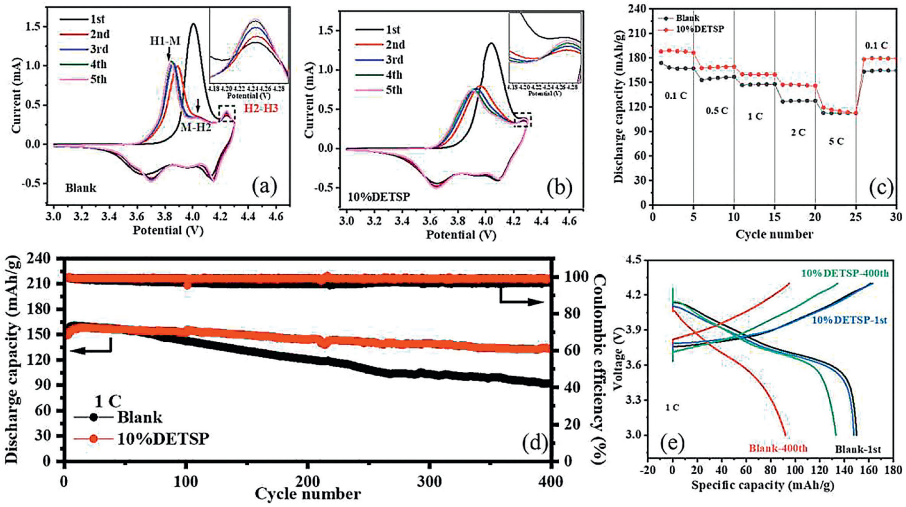

Fig. 2. CV curves of NCM811/Li half cells with (a) blank electrolyte and (b) 10% DETSP electrolyte. (c) Rate performance, (d) long-term cycling performance at 1 C, and (e) corresponding charge/discharge profiles of NCM811/Li half cells with different electrolytes.

S1 (Supporting information). The ion conductivities of electrolytes with 5% and 10% of DETSP were 0.67 and 0.57 mS/cm, respectively, lower than that of the blank electrolyte (1.28 mS/cm), while their electrochemical windows were 4.2 V, same as that of the blank electrolyte. However, further increasing the content of DETSP to 15% made the serious deterioration of both ion conductivity and electrochemical window. Based on these above results, comprehensively considering the flame retardancy and electrochemical properties, the electrolyte with 10% DETSP was chosen to investigate the performance of LIBs subsequently.

The influence of DETSP on the high-voltage cathode (NCM811) was studied firstly. Usually, there are three typical peaks in the CV curve of NCM811 cathode, corresponding to three phases transitions of NCM811 [43]. Specifically, the peaks at approximately 3.86, 4.03, and 4.24 V are assigned to the phase transitions of hexagonal (H1) to monoclinic (M) (H1-M), M to hexagonal (H2) (M-H2), and H2 to hexagonal (H3) (H2-H3), respectively. Among them, the H2-H3 transition is the crucial reason for serious lattice volume variation to sharply decrease the capacity of NCM811 [44,45]. At the 1st cycle, the onset oxidation potential of the blank electrolyte was 3.81 V (Fig. 2a), slightly higher than that of the 10% DETSP electrolyte (Fig. 2b), indicating that the DETSP has higher oxidation activity than the blank electrolyte, which is consistent with its higher energy level of DETSP' HOMO [13]. Interestingly, from the 1st to the 5th cycle, the H2-H3 transition peak of NCM811 for the 10% DETSP electrolyte was weak with little change in intensity, while that of the blank electrolyte was strong and gradually increased, indicating that the DETSP can significantly inhibit the H2-H3 phase transition. Correspondingly, for DETSP-containing electrolyte and blank electrolyte during discharge, their peaks of phase transition from H3 to H2 (H3-H2) at about 4.1 V presented a similar changing rule to that of H2-H3 phase transition. These results indicate that the preferential oxidation of DETSP in electrolyte is conducive to construct a stable cathode-electrolyte interface (CEI) on the NCM811 and further suppress the NCM811 phase transition during the charge-discharge process, which would endow a good cycling performance for the high-voltage LIBs.

As expected, it can be found in Fig. 2c that the NCM811/Li cell with 10% DETSP electrolyte delivered a higher discharge specific capacity than that of the cell using blank electrolyte at current densities from 0.1 C to 5 C, and the capacity can return to as high as 178.5 mAh/g at 0.1 C after cycling at 5 C. Beyond that, the long-term cycling tests (Fig. 2d) at 1 C show that the 10% DETSP electrolyte-based NCM811/Li cell possessed an average Coulombic efficiency of 99.3% and a capacity retention of 89.9% after 400 cycles, while those of the blank electrolyte were only 96.9% and 61.3%, respectively. As is well-known, the voltage is one of the most essential parameters for energy density, and the irreversibility of the NCM phase transition usually leads to a decrease of discharge voltage [45]. According to the charge/discharge curves (Fig. 2e), the polarization voltage of 10% DETSP electrolyte-based cell was noticeably low throughout the long-term cycling (Fig. S2 in Supporting information), but the polarization voltage of the cell using the blank electrolyte dramatically increased with the cycling times. Overall, it can be concluded that the NCM811/Li cell can achieve the excellent long-term cycling stability by adding DETSP to the commercial electrolyte.

As an important parameter for the interfacial compatibility, the interfacial impedance plays a significant role in studying the electrochemical performance [46]. The electrochemical impedance spectra of NCM811/Li cells with different electrolytes before and after cycling were illustrated in Figs. S3a and b (Supporting information), respectively, and the relevant parameters from the fitted equivalent circuit models were summarized in Table S2 (Supporting information). Before cycling, the bulk resistance (R_b) of the 10% DETSP electrolyte was close to that of the blank electrolyte, but its charge transfer resistance (R_{ct}) at the interface was much less than that of the blank electrolyte. After 100 cycles at 1 C, although the resistance of Li^+ transport through the interface (R_f) of the two electrolytes was almost the same, the R_{ct} values of the 10% DETSP electrolyte and the blank electrolyte increased to 274.7 and 525.7 Ω, respectively. These results suggest that DETSP is beneficial to decrease the resistance and improve interfacial stability between the NCM811 cathode and the electrolyte.

The structural and morphological degradation of NCM811 like corrosion and volume expansion is often induced by side reactions between electrolyte and NCM811 cathode during the charge/discharge process. Therefore, the NCM811 cathodes of NCM811/Li cells with different electrolytes before and after 200 cycles were observed by scanning electron microscopy (SEM). As shown in Figs. 3a-f, compared with the fresh NCM811 cathode, the NCM811 particles for the blank electrolyte after cycling were swollen with rough surface, while the NCM811 particles for 10% DETSP electrolyte after cycling exhibited a smooth surface with a relatively intact morphology, indicating its better stability, which probably attributed to the ability of DETSP to scavenge HF. In addi-

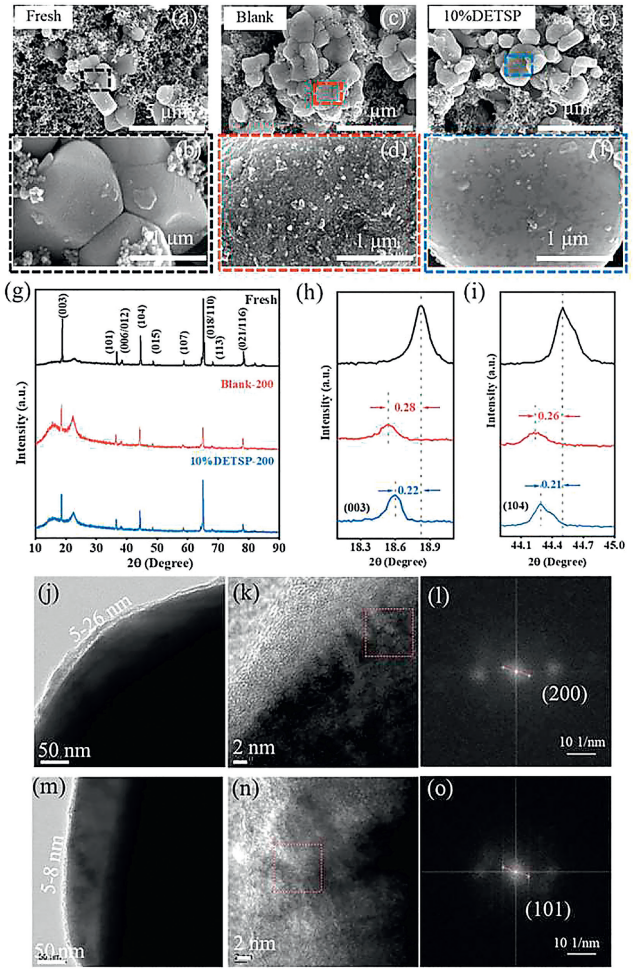

Fig. 3. SEM images of (a, b) fresh NCM811, (c, d) NCM811 cycled in blank electrolyte, and (e, f) NCM811 cycled in 10% DETSP electrolyte after 200 cycles at 1 C. (g) XRD patterns of NCM811 and (h, i) corresponding partially enlarged patterns. TEM images of NCM811 from various electrolytes-based cells after cycling: (j, k) blank electrolyte and (l) corresponding FFT image, (m, n) 10% DETSP electrolyte and (o) corresponding FFT image.

tion, the corresponding Li anode surface was also illustrated in Fig. S4 (Supporting information). Comparing the digital photos in Figs. S4d and g, there were much more deposits on the Li surface of the cell using the blank electrolyte, and high magnifications of SEM further show that there were plenty of cracks in the sediments on the surface and many irregular Li dendrites. However, the cell using 10% DETSP electrolyte had a relatively flat Li surface with only a few cracks and deposits. These results suggest that DETSP can inhibit the side reactions between electrolytes and electrodes, thus reducing continuous electrolyte decomposition and improving the stability of both the NCM811 cathode and Li anode.

The structure of NCM811 was further characterized by X-ray diffraction (XRD). As shown in Fig. 3g, after 200 cycles, the main peaks of NCM811 from two cells with either 10% DETSP electrolyte or blank electrolyte were almost similar to the fresh NCM811. However, compared with the fresh NCM811, for the blank electrolyte after cycling, the corresponding enlarged patterns show that the positions of (003) and (104) peaks of NCM811 shifted to the smaller 2θ angels and their intensities became weaker (Figs. 3h and i), which could be ascribed to the loss of structural order and the expansion of lattice [47]. By contrast, the less shift of 2θ angles and the weaker attenuation of intensities for the (003) and (104) peaks of NCM811 from the 10% DETSP electrolyte-based cell after cycling further demonstrate the improved structural stability of NCM811 [48].

Furthermore, the CEI on the NCM811 was observed by the transmission electron microscopy (TEM). As shown in Figs. 3j and m, a non-uniform CEI with a wide thickness of 5–26 nm is visible for the blank electrolyte, while there is a more uniform and thinner CEI with a thickness of only 5–8 nm for DETSP-containing electrolyte, which is conducive to Li^+ transportation between the cathode and the electrolyte [49]. Higher magnification in Fig. 3k and the corresponding fast Fourier transformed (FFT) image (Fig. 3l) reveal the existence of the (200) of NiO rock-salt phase, demonstrating that the structure of NCM811 has been transformed, which is harmful to the capacity [44]. In contrast, as shown in Figs. 3n and o, the (101) belonging to NCM811 suggests that the NCM811 cathode after cycled in the 10% DETSP electrolyte can remain a relatively pristine crystal structure, which is consistent with the results of XRD. Furthermore, as shown in Fig. S5 (Supporting information), the transition metal (Ni and Mn) contents of Li anodes cycled in different electrolytes were determined by inductively coupled plasma optical emission spectrometry (ICP-OES). The Ni and Mn contents of 10% DETSP electrolyte-based cell are obviously less than those of the blank, indicating that 10% DETSP can effectively suppress transition metal dissolution. These results suggest that the addition of DETSP can produce an ideally stable CEI and suppress severe phase transition of NCM811 during cycling, so as to enhance its structural stability.

To better reveal the role of the DETSP on the interface between the cathode and the electrolyte, the composition of CEI was characterized by X-ray photoelectron spectroscopy (XPS). As shown in Fig. S6 (Supporting information), the peaks of the C–C (284.8 eV), C–H (285.9 eV), and C–O–C (286.9 eV) in the high-resolution C 1s spectra are mainly attributed to the carbonate solvents and polyvinylidene fluoride (PVDF) binder [50]. The peak at 290.0 eV in the C 1s and the peak of C=O at around 534.0 eV in the high-resolution O 1s spectra correspond to the decomposition of carbonate electrolytes. As illustrated in Fig. 4a, the C–F (688.4 eV) and the LiF (685.8 eV) in the high-resolution F 1s spectra can be ascribed to the PVDF binder and the decomposition of $LiPF_6$, respectively [51]. The LiF ratio of 10% DETSP electrolyte is only 32%, which is significantly less than that of the blank electrolyte (62%). Too much LiF could increase the interfacial impedance and badly affect the ion conductivity [14]. Additionally, as the components of a protective film, Li_xPF_y (137.4 eV) and $Li_xPO_yF_z$ (134.6 eV) in the high-resolution P 2p spectra were also produced by the decomposition of the electrolyte. In the high-resolution Si 2p spectra, it is worth noting that the Si-F (104.9 eV) and Si–O (103.1 eV) can be observed on the surface of NCM811 from the cycled cell with the 10% DETSP electrolyte, while there were no significant signals of the electrode cycled in the blank electrolyte. The Si species were derived from the decomposition of DETSP, further indicating that DETSP can induce a protective film on the surface of NCM811, leading to less electrolyte decomposition and structural loss of cathode.

To better explain the mechanism of DETSP on the improved electrochemical performance, the different electrolytes added with 5 vol% H_2O for several hours were investigated by NMR analysis. As shown in Fig. 4b, the ^{31}P NMR spectra show that there was a new peak of $PO_xF_y^-$ at around −15 ppm appeared in the blank electrolyte after hydrolysis, while only the peaks of $LiPF_6$ were detected in the 10% DETSP electrolyte. Moreover, the ^{19}F NMR spectrum of the hydrolyzed blank electrolyte also displayed the peak of $PO_xF_y^-$ at around −72 ppm and a new peak at −144 ppm assigned to HF (Fig. 4c). However, both peaks disappeared in the 10% DETSP electrolyte, indicating that the DETSP can inhibit the hydrolysis of electrolytes, reducing the formation of fluorine-containing products like $PO_xF_y^-$ and HF to avoid the further leaching of transition metal ions from NCM811 [50], which ensures to re-

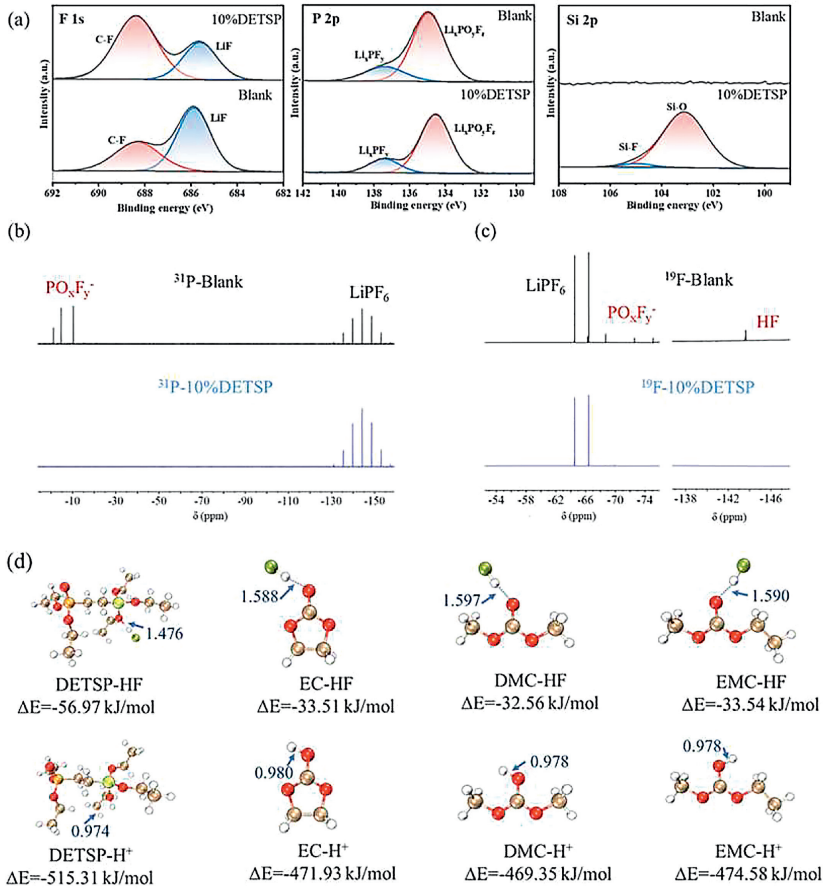

Fig. 4. (a) XPS spectra of NCM811 extracted from cells with different electrolytes after 200 cycles. (b) ^{1}H NMR and (c) ^{19}F NMR spectra of the blank electrolyte and 10% DETSP electrolyte after hydrolysis. (d) Binding energies of X-HF and X-H$^+$ (X = DETSP, EC, DMC, and EMC).

main the relatively complete surface of NCM811 during charge and discharge.

In addition, the binding energies of DETSP with HF/H$^+$ were investigated by DFT calculations. It can be seen from Fig. 4d that DETSP tends to combine with HF and the binding energy is −56.97 kJ/mol, lower than those of the carbonated solvents, indicating that DETSP could eliminate negative effects of HF on electrodes [50,51]. And the binding energy of DETSP with H$^+$ is also the lowest compared with the other components of electrolytes. The calculation results are in agreement with the hydrolysis experiment, suggesting that DETSP is conducive to capturing the hazardous products from the side reactions of electrolytes.

To expand applications of DETSP, the compatibility of 10% DETSP electrolyte with graphite (GP) was studied. As shown in Fig. S7 (Supporting information), during the first cycle, the reduction peak area of the GP/Li cell with 10% DETSP electrolyte at around 0.7 V was larger than that of the blank electrolyte, indicating that DETSP would probably be involved in the reduction reaction. The rate performance of GP/Li cells using different electrolytes was illustrated in Fig. 5a, and it can be seen that adding 10% DETSP did not affect the discharge specific capacity, and the cell still remained at comparable capacities to those of the blank electrolyte at current densities from 0.2 C to 5 C. Significantly, the capacity of cell with 10% DETSP electrolyte can return to a level as high as that of the blank electrolyte, indicating its excellent rate performance. Furthermore, the cycling test at 0.5 C shows that the cell with 10% DETSP electrolyte had almost no capacity decay after 150 cycles (Fig. 5b). More interestingly, both capacity and Coulombic efficiency of cell using 10% DETSP electrolyte were far higher than those of the cell using blank electrolyte during the initial 10 cycles, indicating that DETSP may promote the production of a stable interface on the GP anode. Actually, it can be found from Fig. S8 (Supporting information) that 10% DETSP electrolyte-based GP half cells had a stable first charge-discharge curve and a lower polarization voltage. Unlike some conventional phosphate flame retardants, these results indicate that DETSP as the functional additive of blank electrolyte is highly compatible with the GP anode.

For evaluating practicality of DETSP, the cycling performance of NCM811/GP full cells was conducted at 0.5 C. It can be seen from Fig. 5c that the NCM811/GP full cell with the 10% DETSP electrolyte exhibits a better cycling stability than the full cell with the blank electrolyte. Specifically, after 100 cycles, the former delivered a capacity retention of 73.5%, while the latter's capacity retention was only 53.9%. The corresponding charge/discharge profiles in Fig. 5d show that the intersection of the cell with 10% DETSP electrolyte shifted right, indicating that DETSP could reduce the polarization at the interfaces between electrolytes and electrodes [52].

The differential scanning calorimetry (DSC) was carried out to investigate the influence of DETSP on the thermal behavior of NCM811/Li cells (state of charge (SOC) = 100%) [22]. As shown in Fig. 5e, there were two exothermic peaks around 176 and 187 °C in the cell with the blank electrolyte, corresponding to the reaction with Li metal and the decomposition of electrolyte, respectively. The total specific heat release was as high as 1322 J/g, while that of the 10% DETSP-based cell was only 465 J/g, suggesting that 10% DETSP can improve the safety of cells. It is worth noting that the endothermic peak of the cell with 10% DETSP electrolyte was assigned to the melting of Li metal (Fig. 5f), while this peak was

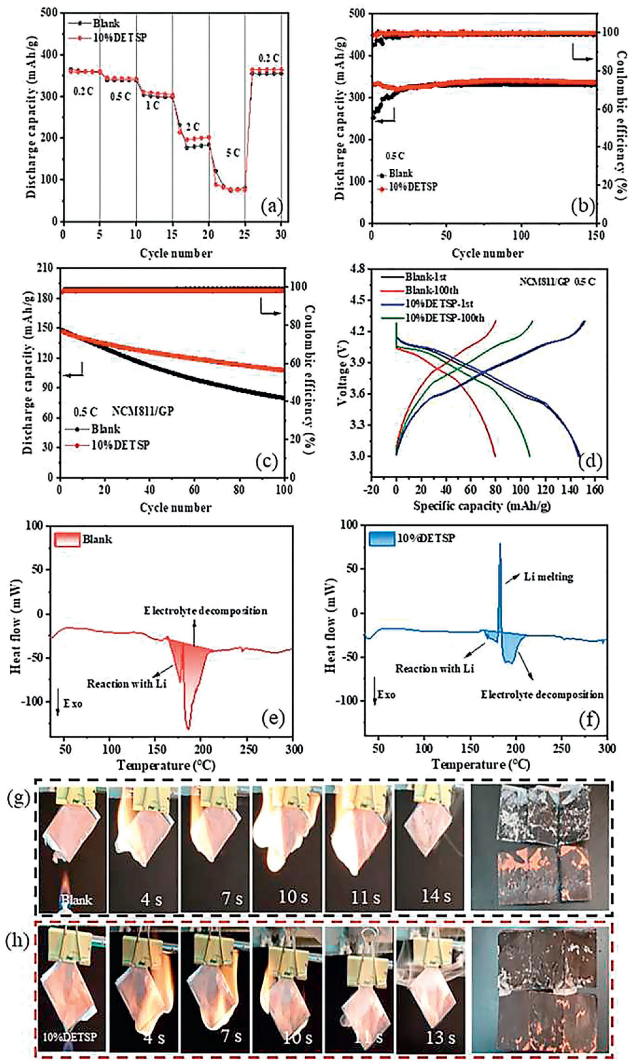

Fig. 5. (a) Rate performance and (b) cycling performance at 0.5 C of GP/Li half cells. (c) Cycling performance at 0.5 C and (d) corresponding charge/discharge profiles of NCM811/GP full cells with different electrolytes. DSC of NCM811/Li cells with (e) blank electrolyte and (f) 10% DETSP electrolyte. Burning tests of pouch batteries and the corresponding digital photos of electrodes after burning with (g) blank electrolyte and (h) 10% DETSP electrolyte.

invisible and replaced by the excessively large exothermic peaks in the cell with blank electrolyte, further indicating that DETSP can reduce the risk of thermal runaway of cells.

Furthermore, the burning test of pouch battery with the blank electrolyte and the corresponding digital photos of electrodes after ignition were illustrated in Fig. 5g. The combustion process lasted 14 s with damaged electrodes and significant active material loss. In contrast, for the pouch battery with 10% DETSP electrolyte (Fig. 5h), it can be seen that the flame was extinguished after 11 s, and the surface of the electrodes after combustion was relatively complete, suggesting that the addition of DETSP shortened the burning time and improved the safety of pouch batteries. Moreover, the composition of the GP anode after burning was characterized by XPS. As shown in Fig. S9 (Supporting information), there were more C in the residue for the 10% DETSP electrolyte, and the Si-O signal was detected, indicating that DETSP may conduce to form barrier char layer in the condensed phase.

In this study, a multifunctional additive DETSP of commercial organic electrolyte was successfully prepared to attain the safe and high-performance high-voltage LIBs. With the addition of 10 wt% DETSP, the SET and heat of combustion decreased nearly half, significantly improving the safety of electrolytes. On the other hand, different from conventional phosphorus flame retardants, the electrochemical properties including electrochemical window and ion conductivity of 10% DETSP electrolyte were comparable to those of the blank electrolyte. Furthermore, the 10% DETSP electrolyte significantly improved the cycling performance of NCM811 with the Coulombic efficiency of 99.3% and the capacity retention of 89.9% after 400 cycles at 1 C. Theoretical calculations and experimental results indicate that DETSP not only can be oxidized preferentially to form a stable protective film but also scavenge HF to avoid structural degradation during cycling. And the 10% DETSP did not reduce the cycling stability of GP anode, even improving the Coulombic efficiency.

Declaration of competing interest

The authors declare no conflict of interest.

Acknowledgments

This work was supported by the National Natural Science Foundation of China (No. 51773134), the Sichuan Science and Technology Program (No. 2019YFH0112), the Fundamental Research Funds for the Central Universities, Institutional Research Fund from Sichuan University (No. 2021SCUNL201), and the 111 Project (No. B20001).

Supplementary materials

Supplementary material associated with this article can be found, in the online version, at doi:10.1016/j.cclet.2023.109123.

References

[1] M.C. Long, G. Wu, X.L. Wang, Y.Z. Wang, Energy Storage Mater. 53 (2022) 62–71.
[2] Y. Gan, M. Liu, R. Tan, et al., Adv. Energy Mater. 12 (2022) 2202779.
[3] Y. Li, G. Zhang, B. Chen, et al., Chin. Chem. Lett. 33 (2022) 3287–3290.
[4] Y. Zhu, X. Luo, H. Zhi, et al., J. Mater. Chem. A 6 (2018) 10990–11004.
[5] H. Maleki Kheimeh Sari, X. Li, Adv. Energy Mater. 9 (2019) 1901597.
[6] Z. Wang, H. Zhu, H. Yu, et al., Chin. Chem. Lett. 34 (2023) 107718.
[7] F. Zhang, Y. Liang, Z. Ye, et al., Chin. Chem. Lett. 35 (2024) 108655.
[8] H.H. Ryu, K.J. Park, C.S. Yoon, Y.K. Sun, Chem. Mater. 30 (2018) 1155–1163.
[9] S.S. Zhang, J. Energy Chem. 41 (2020) 135–141.
[10] Q. Zheng, Y. Yamada, R. Shang, et al., Nat. Energy 5 (2020) 291–298.
[11] S.H. Lee, C.S. Yoon, K. Amine, Y.K. Sun, J. Power Sources 234 (2013) 201–207.
[12] L. Liang, G. Hu, F. Jiang, Y. Cao, J. Alloys Compd. 657 (2016) 570–581.
[13] H.Q. Pham, M. Mirolo, M. Tarik, M. El Kazzi, S. Trabesinger, Energy Storage Mater. 33 (2020) 216–229.
[14] J. Liu, X. Song, L. Zhou, et al., Nano Energy 46 (2018) 404–414.
[15] S.T. Myung, F. Maglia, K.J. Park, et al., ACS Energy Lett. 2 (2017) 196–223.
[16] W. Qiu, J. Xia, L. Chen, J.R. Dahn, J. Power Sources 318 (2016) 228–234.
[17] S. Li, T. Yang, W. Wang, et al., Electrochim. Acta 352 (2020) 136492.
[18] H. Liu, A.J. Naylor, A.S. Menon, et al., Adv. Mater. Interfaces 7 (2020) 2000277.
[19] Y.M. Song, J.G. Han, S. Park, K.T. Lee, N.S. Choi, J. Mater. Chem. A 2 (2014) 9506–9513.
[20] C. Ye, W. Tu, L. Yin, et al., J. Mater. Chem. A 6 (2018) 17642–17652.
[21] Z. Ren, H. Qiu, C. Fan, et al., Adv. Funct. Mater. 33 (2023) 2302411.
[22] M.C. Long, T. Wang, P.H. Duan, et al., J. Energy Chem. 65 (2022) 9–18.
[23] L. Han, C. Liao, Y. Liu, et al., Energy Storage Mater. 52 (2022) 562–572.
[24] T. Zhu, G. Liu, D. Chen, et al., Energy Storage Mater. 50 (2022) 495–504.
[25] B. Wang, Y. Wu, S. Zhuo, et al., J. Mater. Chem. A 8 (2020) 5968–5974.
[26] Y. Kato, S. Hori, T. Saito, et al., Nat. Energy 1 (2016) 16030.
[27] L. Zhou, T.T. Zuo, C.Y. Kwok, et al., Nat. Energy 7 (2022) 83–93.
[28] Q. Wang, L. Jiang, Y. Yu, J. Sun, Nano Energy 55 (2019) 93–114.
[29] X. Tian, Y. Yi, B. Fang, et al., Chem. Mater. 32 (2020) 9821–9848.
[30] P. Jaumaux, J. Wu, D. Shanmukaraj, et al., Adv. Funct. Mater. 31 (2021) 2008644.
[31] R.P. Dunn, J. Kafle, F.C. Krause, et al., J. Electrochem. Soc. 159 (2012) A2100.
[32] X.L. Yao, S. Xie, C.H. Chen, et al., J. Power Sources 144 (2005) 170–175.
[33] L. Jiang, C. Liang, H. Li, Q. Wang, J. Sun, ACS Appl. Energy Mater. 3 (2020) 1719–1729.
[34] Z. Zeng, B. Wu, L. Xiao, et al., J. Power Sources 279 (2015) 6–12.
[35] Q.S. Liu, Y.Z. Quan, M.C. Liu, et al., J. Energy Chem. 83 (2023) 239–246.
[36] Y.Z. Quan, Q.S. Liu, M.C. Liu, et al., J. Energy Chem. 84 (2023) 374–384.

[37] R. Chen, Y. Zhao, Y. Li, et al., J. Mater. Chem. A 5 (2017) 5142–5147.
[38] H.P. Zhang, Q. Xia, B. Wang, et al., Electrochem. Commun. 11 (2009) 526–529.
[39] L.L. Li, L. Li, B. Wang, et al., Electrochim. Acta 56 (2011) 4858–4864.
[40] D. Lu, S. Zhang, J. Li, et al., Adv. Energy Mater. 13 (2023) 2300684.
[41] Q. Wang, B. Mao, S.I. Stoliarov, J. Sun, Progr. Energy Combust. Sci. 73 (2019) 95–131.
[42] K. Xu, M.S. Ding, S. Zhang, J.L. Allen, T.R. Jow, J. Electrochem. Soc. 149 (2002) A622.
[43] T. He, Y. Lu, Y. Su, et al., ChemSusChem 11 (2018) 1639–1648.
[44] J. Yang, Y. Xia, ACS Appl. Mater. Interfaces 8 (2016) 1297–1308.
[45] J. Yang, X. Liu, Y. Wang, et al., Adv. Energy Mater. 11 (2021) 2101956.
[46] M.C. Liu, H.J. Chen, G. Wu, X.L. Wang, Y.Z. Wang, Chin. Chem. Lett. 34 (2023) 107546.
[47] P.P. Wang, F.J. Yang, J. Bai, et al., J. Power Sources 509 (2021) 230361.
[48] S. Zhang, F. Sun, X. Du, et al., Energy Environ. Sci. 16 (2023) 2591–2602.
[49] S. Zhang, X. Zhuang, X. Du, et al., Adv. Mater. 35 (2023) 2301312.
[50] Y. Li, K. Wang, J. Chen, et al., ACS Appl. Mater. Interfaces 12 (2020) 28169–28178.
[51] H. Chen, J. Chen, W. Zhang, et al., J. Mater. Chem. A 8 (2020) 22054–22064.
[52] Z. Li, C. Qiu, Y. Lin, et al., Ind. Eng. Chem. Res. 61 (2022) 4842–4849.